


RESEARCH ARTICLE

Open Access



The message of oldhamites from enstatite chondrites

Tahar Hammouda^{1*} , Maud Boyet¹, Paul Frossard¹ and Camille Cartier²

Abstract

We have determined rare-earth element (REE) abundances in oldhamites (CaS) from 13 unequilibrated and equilibrated enstatite chondrites (5 EH and 8 EL) and in a few enstatites by in situ, laser ablation ICP-MS. In EH chondrites, oldhamite REE patterns vary from the most primitive petrographic types (EH3) to the most metamorphosed types (EH5). In EH3, Cl-normalized REE patterns are convex downward with strong positive Eu and Yb anomalies, whereas EH5 display flat patterns with enrichments reaching about 80 times Cl abundances. The positive anomalies of Eu and Yb found in oldhamites of primitive EH chondrites indicate that they represent the condensation of a residual gas fraction, in a manner similar to fine-grained CAIs of carbonaceous chondrites. The early condensate may have been preserved in the matrix of unequilibrated EH. Equilibrated EH oldhamite patterns may result from metamorphic evolution and REE redistribution on the EH parent body. On the contrary, all the oldhamites from EL chondrites (EL3 to EL6) display a single kind of patterns, which is convex upward and is about 100 times enriched relative to Cl, with a negative Eu anomaly. In addition, the EL pattern is similar to that of oldhamites from aubrites (enstatite achondrites). The latter observation suggests that oldhamites of all EL metamorphic types (including primitive ones) bear the signature of a magmatic event accompanied by FeS loss as vapor, prior to the assembly of the EL parent body. Given the difficulty of obtaining precise ages on enstatite chondrites, it is not possible to discuss the chronology of the events recorded by the oldhamite REE patterns.

Keywords: Enstatite chondrite, Oldhamite, Rare-earth-elements, Redox conditions, Condensation, Vaporization

1 Introduction

Enstatite chondrites (EC) represent the most reduced type of chondrites. Although rare (about 0.6% of total known meteorites, Krot et al. 2014; Weisberg and Kimura 2012), EC are of great interest because they share many isotopic characteristics with terrestrial samples [oxygen (Clayton 1993), nitrogen (Javoy et al. 1986; Cartigny et al. 1997), molybdenum (Dauphas et al. 2002; Burkhardt et al. 2011), chromium (Trinquier et al. 2007); titanium (Trinquier et al. 2009); Xe and Kr (Miura et al. 2007); nickel (Regelous et al. 2008)] and it has been suggested that they could represent the major building blocks of our planet

(Javoy 1995; Javoy et al. 2010). Enstatite chondrites are divided into two groups, EH and EL, which differ by their bulk iron and sulfur contents (H = high; L = low, Wasson and Kallemeyn 1988; Krot et al. 2014). The two groups also differ in their sulfide mineralogy. In addition to troilite (FeS), daubréelite (FeCr₂S₄) and oldhamite (CaS) are common to both groups, whereas niningerite ((Mg,Fe)S) is the diagnostic sulfide of EH chondrites and alabandite ((Mn,Fe)S) is specific to EL (Lin and El Goresy 2002). The presence of unusual sulfides containing normally lithophile elements (Mg, Ca, Mn, Ti, Na), Si-bearing kamacite, nitrides, phosphides and carbides reflects highly reducing environment of EC formation. Under these conditions, elements including the rare-earth elements (REE) and the actinides that are lithophile in terrestrial conditions and in other types of chondrites tend to be siderophile and/or chalcophile (e.g., Barrat et al. 2014; Crozaz

*Correspondence: tahar.hammouda@uca.fr

¹ CNRS, IRD, OPGC, Laboratoire Magmas et Volcans, Université Clermont Auvergne, 63000 Clermont-Ferrand, France
Full list of author information is available at the end of the article

and Lundberg 1995; Gannoun et al. 2011; Piani et al. 2016; Cartier and Wood 2019; Anzures et al. 2020).

Oldhamite has attracted much attention because of its rare-earth element content. Previous studies have shown that this phase can carry about half of the EC REE budget, with abundances up to 100 times the chondritic values (Crozas and Lundberg 1995; Gannoun et al. 2011). Because these elements are highly refractory and large ion REEs substitute for Ca in condensates (Lodders 2003; Wood et al. 2019), these observations suggest that oldhamites were formed early by condensation. They can be compared to minerals found in calcium-aluminum rich inclusions (e.g., perovskite and hibonite), which are first to condense from the cooling of a solar gas (Lodders and Fegley 1993). Thermodynamical modeling of condensation at more reducing conditions (C/O ratio >0.5 , Lodders and Fegley 1993; Ebel and Alexander 2011) predicts a sequence in which oldhamite appears during cooling and condensation. Furthermore, at reduced conditions, the models predict that rare-earth elements are incorporated into oldhamite with a final pattern characterized by negative Eu, Yb, and Sm anomalies, because those elements have the lowest condensation temperature among the REE (Lodders and Fegley 1993; see Fig. 1). Instead, oldhamites from primitive EH (Crozas and Lundberg 1995; Gannoun et al. 2011) show positive Eu, Yb, and Sm anomalies. This observation is at odds with a postulated condensation origin for the sulfides of primitive EH at reduced conditions.

Experimental studies on CaS/melt REE partitioning successfully predict positive Eu and Yb anomalies

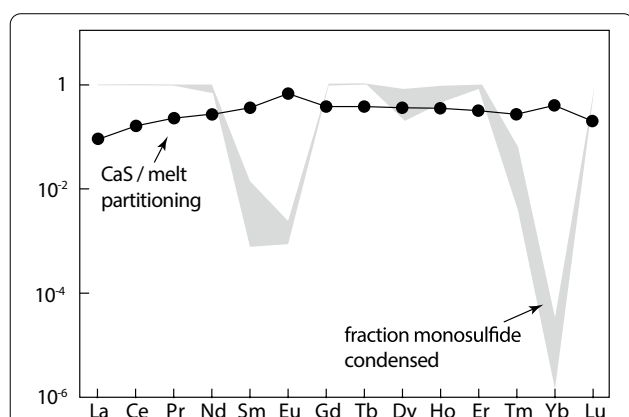


Fig. 1 Rare-Earth Element pattern (in grey) predicted by modeling condensation as monosulfides solid solution in oldhamite [CaS, Lodders and Fegley (1993)]. Conditions are $T = 1378.6$ K (0.1 K below oldhamite condensation temperature) and a nebular gas with $C/O = 1.2$ (reduced conditions). Also shown are the CaS/melt REE partition coefficients determined experimentally by Ingrao et al. (2019)

as observed in primitive EH chondrites (Lodders 1996; Dickinson and McCoy 1997; Ingrao et al. 2019). However, experimental partition coefficient values are of the order of 1 (Fig. 1), which makes it difficult to explain the high REE enrichment in oldhamite, unless a complex magmatic history is considered.

Rare-earth element patterns of oldhamites differ when different groups and metamorphic types are compared (Crozas and Lundberg 1995; Gannoun et al. 2011). These differences may concern overall REE concentrations, the presence or absence of anomalies in the REE patterns, e.g., Eu, Yb, and Sm, as well as the sign of the anomalies. However, literature data are too scarce to fully understand these chemical signatures. Literature data also present information on enstatite compositions (Hsu and Crozas 1998; Gannoun et al. 2011), which show different types of REE patterns. In order to get further insight into the formation conditions of enstatite chondrites as well as to their REE budgets, we have analyzed oldhamites and a few enstatites from a collection of enstatite chondrites that covers most of known types (EH3 to EH5 and EL3 to EL6). We used laser ablation ICP-MS for in situ analysis. With this method, we can relate the textural location to the mineral composition, which is not possible when using the stepwise dissolution techniques (Boyet and Gannoun 2013; Barrat et al. 2014). Thus, we can also discuss the respective advantages of each method, as well as their complementary nature.

2 Methods

2.1 Samples

We studied a collection of both groups of EC with metamorphic grades ranging from type 3 (primitive or unequilibrated) to type 6 (highly equilibrated). With metamorphic grade, from type 3 to type 6, chondrules become progressively less visible, the matrix proportion decreases and minerals become chemically more homogeneous. A detailed list of the studied material is presented in Table 1. We have studied 5 samples from the EH group (2 EH3, 1 EH4, 2 EH5) and 13 from the EL group (6 EL3, 1 EL4/5, 1 EL5, 5 EL6) including both fall and find samples. All EH were suitable for CaS analysis. For EL, 3 EL3 and 2 EL6 yielded no fresh oldhamites and we obtained data for 3 EL3, 1 EL4/5, 1 EL5 and 3 EL6. For each sample, we studied only one section. In the discussion, we also considered Sahara 97,072 and ALHA77295 EH3 from Gannoun et al. (2011).

Meteorite fragments or slabs were mounted in epoxy resin and polished using diamond paste under ethanol. In case the material was already a resin mount, we simply polished it, in order to have a clean surface. In all cases, this preparation allowed for the petrographic observations and subsequent in-situ analyses. For laser ablation,

Table 1 List of samples analyzed minerals in this study

Meteorite	Type	Fall/find	Source	Oldhamite	Enstatite	In-situ REE measurements	Whole rock and leaching
ALHA77295	EH3	Find	NASA		x	[4]	[4]
Caleta el Cobre 025	EH3	Find	J. Gattacceca, CEREGE	x			
Sahara 97096 ^a	EH3	Find	L. Labenne		x	[4]	[4]
Sahara 97158 ^a	EH3	Find	L. Labenne	x		[4]	[4], [6]
Abee	EH4	Fall	L. Labenne	x	x	[3], [2]	[6], [7]
Oudiyat Sbaa	EH5	Find	A. Irving, University of Washington, Seattle	x			
St. Mark's	EH5	Fall	Smithsonian, USNM 3027			[3]	[6], [7]
MAC 88136 ^b	EL3	Find	NASA	x		[1], [3]	[6]
MS 17 ^c	EL3	Fall	S. Haberer, Haberer Meteorite	x			
MS 189 ^c	EL3	Fall	A. Black, Impatika	x			
MS 196 ^c	EL4/5	Fall	A. Black, Impatika	x			
Adrar Bous	EL5	Find	L. Labenne	x	x		[7]
Atlanta	EL6	Find	A. El Goresy, BGI	x	x		
Hvittis	EL6	Fall	J. Schooler	x	x		[6], [7]
NWA 974	EL6	Find	Fectay				[6]

Previous studies providing data on rare-earth elements (in-situ and whole-rock) on these samples are indicated in bracket []

[1] Crozaz and Lundberg (1995): oldhamite, enstatite and niningerite by SIMS

[2] Hsu (1998): albite by SIMS

[3] Hsu and Crozaz (1998): enstatite by SIMS

[4] Gannoun et al. (2011): oldhamite by SIMS and LA-ICPMS, enstatite and niningerite by SIMS, whole-rock measurements

[5] Boyet and Gannoun (2013): step-wise dissolution techniques, measurement of leachings and residues

[6] Barrat et al. (2014): whole-rock, leachate and residue measurements

[7] Boyet et al. (2018): whole-rock measurements

^a Sahara 97072, 97096 and 97158 are paired meteorites

^b Paired to MAC 88180

^c MS samples are fragments of the polymict breccia of Almahata Sitta fall

the principal limitation is the grain size. This is particularly true for elements with low abundances, because large spots are needed in order to obtain enough counts on the detectors. In addition, those minerals that showed clear evidence of alteration, such as rust or voids, were discarded.

Except for NWA 974 (EL6), all meteorites studied here have been subject to previous investigations, either for mineralogy and/or whole rock composition. Reports of whole rock major and trace elements can be found in Keil (1968), Kallemeyn and Wasson (1986), Gannoun et al. (2011), Barrat et al. (2014) and Boyet et al. (2018). Individual mineral major element concentrations obtained using electron microprobe have been published (Keil 1968; Buseck and Holdsworth 1972; Rubin 1983; Sears et al. 1984) with detailed studies on metal and troilite (Keil 1969; Zhang and Sears 1996; Piani et al. 2016, Weyrauch et al. 2018). Trace elements in sulfides have been reported by Floss et al. (1990), Floss and Crozaz (1993), Crozaz and Lundberg (1995), Hsu and Crozaz (1998), Gannoun et al. (2011) and El Goresy et al. (2017).

2.2 Petrographic observations and major and minor element analysis

Petrographic observations were performed using a JEOL scanning electron microscope (JSM-5910LV) operating at 15 kV. Major element analyses of minerals were obtained using an SX100 electron microprobe using a focused beam, with a 15 kV accelerating voltage, and a 15 nA beam current. For sulfide analyses, we used pyrite (FeS₂) as a standard for Fe and S, metals for Mn, and Ni, wollastonite for Ca, San Carlos olivine for Mg, Cr₂O₃ for Cr and MnTiO₃ for Ti. Counting times on peak were 20 s for Fe, Mg and S, and 10 s for Ca, Ni, Mn, Cr and Ti.

2.3 In-situ trace element analysis

Trace element concentrations in oldhamites and enstatites were obtained using an Agilent 7500-cs or a Thermo Fisher Element XR ICP-MS, coupled with a Resonetics M-50 laser at Laboratoire Magmas et Volcans. The laser was operated at 193 nm wavelength with energy varying between 2 and 8 mJ, depending on the nature and size of the phase of interest. We used 3 Hz frequency and

nominal laser spot size of 20 μm for oldhamite and up to 100 μm for enstatite. In order to improve detection limits and counting statistics, we used block counting times of 60 ms. For major elements, we used 2, 10 or 20 ms. Total ablation duration was usually about 80 s and was done in pure He atmosphere. The analyte was carried to the ICP torch by a gas mixture wherein $\text{N}_2 + \text{Ar}$ were added to He. We used the following gas flows: He, 750 ml/min; N_2 , 7 ml/min; Ar nebulizer gas, 0.88 l/min; Ar cool gas, 15 l/min; Ar auxiliary gas, 1 l/min. Plasma RF was 1300 W. NIST 610 glass standard (values from Gagnon et al. 2008) was used for calibration of relative sensitivities. Analyses were normalized using average Ca and Mg concentrations determined by electron microprobe for oldhamite and enstatite, respectively. NIST 612 and BCR glasses were used as secondary standards. Trace-element concentration reductions were done with the GLITTER software (van Achterberg et al. 2001). Accuracy on external standards from the instruments has been discussed recently (Hammouda et al. 2010; Cartier et al. 2014). All analyzed elements are accurate within 10% except for Nb (less than 15%) versus Gagnon et al. (2008) and Ti (less than 20%) versus Pearce et al. (1997).

3 Results

3.1 Description of oldhamite occurrences

The petrographic texture of some EH chondrite sections studied is illustrated in Fig. 2. In unequilibrated EH3 (such as Sahara 97158), oldhamite occurs in metal and sulfide aggregates as well as isolated grains in the matrix. Grain size ranges between less than 10 μm to more than 100 μm (Fig. 2a, b). Gannoun et al. (2011) reported similar descriptions and images for oldhamites of the paired meteorite Sahara 97072. In Abee (EH4, impact-melt breccia), oldhamite grains are disseminated in the matrix (Fig. 2c). They can also be found as intergrowths with enstatite (Fig. 2d). Grain sizes range between a few to 100 μm . In St. Mark's (EH5), oldhamite grains are present in the matrix (Fig. 2e) but chondrules consisting of an intergrowth of oldhamite, troilite and enstatite are frequent (Fig. 2f). In both cases, oldhamite grains can reach 100 μm .

Oldhamites of some of the EL chondrites studied are illustrated in Fig. 3. In unequilibrated EL3 (MS 189, MAC 88136), oldhamite grains are disseminated in the matrix (Fig. 3b, c). One chondrule in MS 189 consists of a radial intergrowth of oldhamite, troilite, and enstatite (Fig. 3a). In EL5 (Adrar Bous), oldhamite grains are disseminated in the matrix (Fig. 3d, e). Their size is usually small (less than 10 μm) but some larger grains of a few tens of μm are present (Fig. 3e). Equilibrated EL6 chondrites (such as Hvittis, Fig. 3f) contain oldhamite grains that can be larger than 100 μm . Some smaller grains (few tens of μm)

are also present. In Hvittis, a chondrule fragment showing a radial intergrowth of oldhamite and enstatite (similar to that found in MS 189) is present.

3.2 Oldhamite major element concentrations

Oldhamites of EH are close to CaS end-member composition, with other components (Fe, Mn, Mg) amounting to less than 1 wt. % each. St. Mark's (EH5) has slightly more Mn and Mg, and slightly less Fe than the EH3 oldhamites. In EH3, Fe is the most abundant cation, after Ca, whereas in EH5, it is Mg. In all cases, Mn concentration is intermediate between Fe and Mg. Finally, Fe is the element with the highest variability.

Oldhamites of EL have less Ca than those of EH. Within each meteorite, oldhamite composition is rather homogeneous, except in EL3, where Fe-poor (0.7 wt.%) and Fe-rich (up to 4 wt.%) grains were found. In Adrar Bous (EL5) Fe is about 1.1 wt.%, whereas in EL6, Fe is lower (0.3 wt.%). It cannot be excluded that high Fe values found in EL3 oldhamite are due to contamination. In EL3, Mn amounts to 0.8 wt.%, and in the other types, Mn concentration ranges between 1.2 and 1.4 wt.%. Mg ranges between 0.18 and 0.24 in EL3 and between 0.4 and 0.6 wt.% in EL 5 and EL6.

Major element concentrations analyzed in oldhamites are provided in the Additional file 1, together with the detection limits.

3.3 Rare-earth element concentrations in oldhamites

Rare-earth element concentrations of oldhamites (averages and 1 sigma standard deviations) are given in Table 2. CI-normalized REE patterns are illustrated in Fig. 4. Individual patterns for all laser shots in each sample are displayed in the Additional file 1. In EH chondrites, CI-normalized REE patterns vary according to metamorphic type. In primitive EH3 (Sahara 97158, Caleta el Cobre 025), oldhamites are characterized by strong positive anomalies for Eu ($4 < \text{Eu}/\text{Eu}^* < 5$), Yb ($2.5 < \text{Yb}/\text{Yb}^* < 3$), and Sm to a lesser extent, whereas the patterns are overall convex downward. Values of $[\text{Eu}]_{\text{N}}$ and $[\text{Yb}]_{\text{N}}$ are about 60 and 40, respectively. All other CI-normalized REE abundance decrease from La to Lu, with values ranging between 46 and 8. These patterns are similar to the C-D type patterns previously reported in the literature for unequilibrated EH3 chondrites (ALHA77295 and Sahara 97072, Gannoun et al. 2011; Qingzhen, Crozaz and Lundberg 1995). Variations between grains in Eu concentration are limited, whereas other REE concentrations (including Yb) spread over about one order of magnitude. Oldhamites from Abee (EH4), St. Mark's and Oudiyat Sbaa (EH5) are homogeneous, within each meteorite. In Abee (EH4-IMB), all analyzed grains display the same CI-normalized

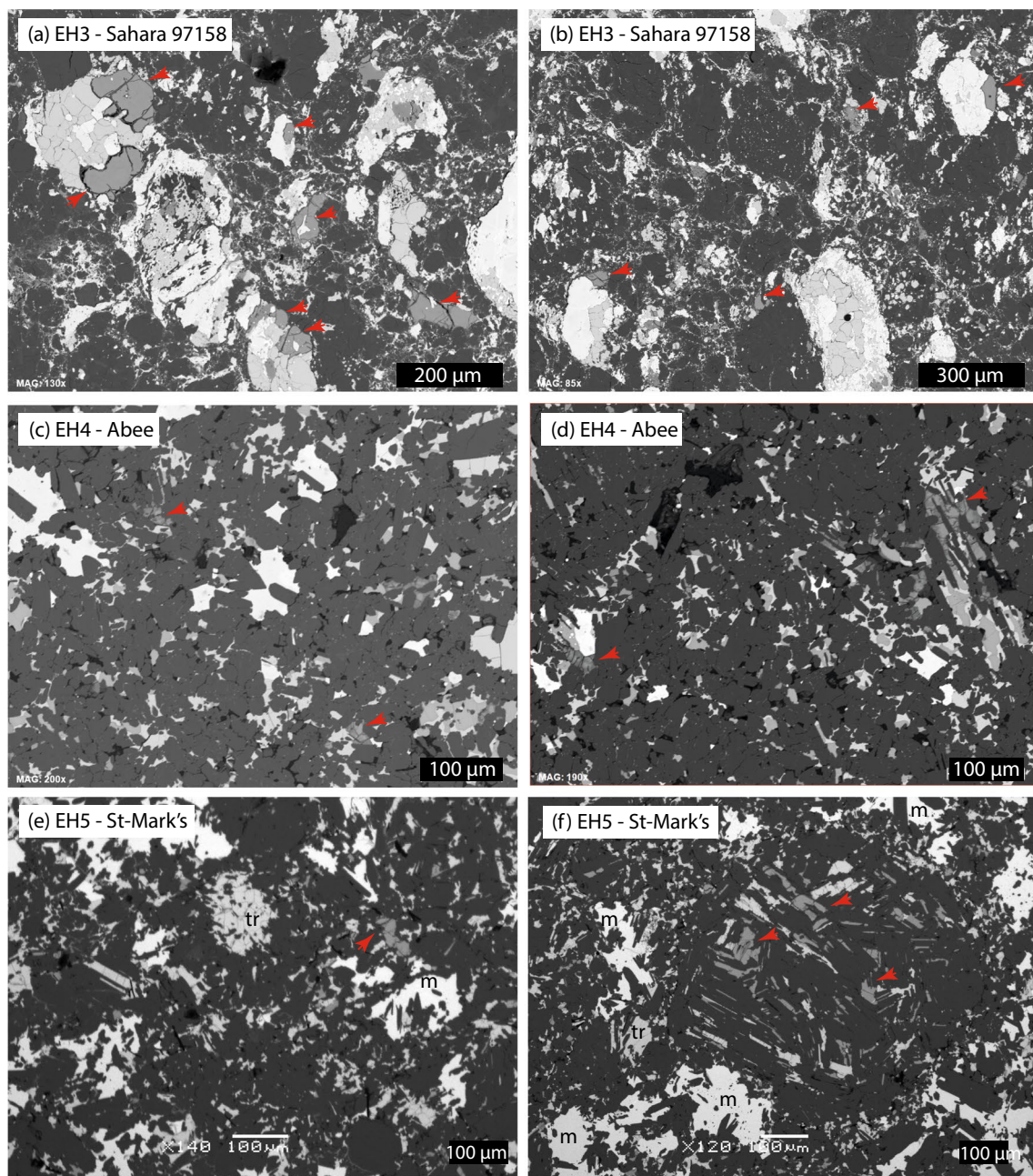


Fig. 2 Scanning electron images of some of the EH samples studied, illustrating the textural position of the oldhamite grains, indicated by the red arrows. Also indicated are the metal (m) and troilite (tr) grains

REE patterns, slightly convex upward, with $[REE]_N$ ranging between 60 and 80, and a negative Eu anomaly ($Eu/Eu^* = 0.66$). In EH5 (St. Mark's and Oudiyat Sbaa), oldhamite CI-normalized REE patterns are flat and no anomaly is observed. $[REE]_N$ range between 60 and 70. Therefore, a major difference between metamorphic types is the presence of strong positive Eu and Yb (and Sm) anomalies in unequilibrated EH3. No positive

Eu and Yb anomalies were found in Abee, St. Mark's, and Oudiyat Sbaa. In Indarch (EH4), Crozaz and Lundberg (1995) found slightly fractionated REE patterns ($[La]_N = 82$; $[Lu]_N = 54$), with little variability. Most of the reported REE patterns in Indarch display a positive Yb anomaly (Yb/Yb^* of about 1.5) and a slight negative Eu anomaly, which is difficult to quantify because of the light rare-earth element (LREE) and heavy rare-earth

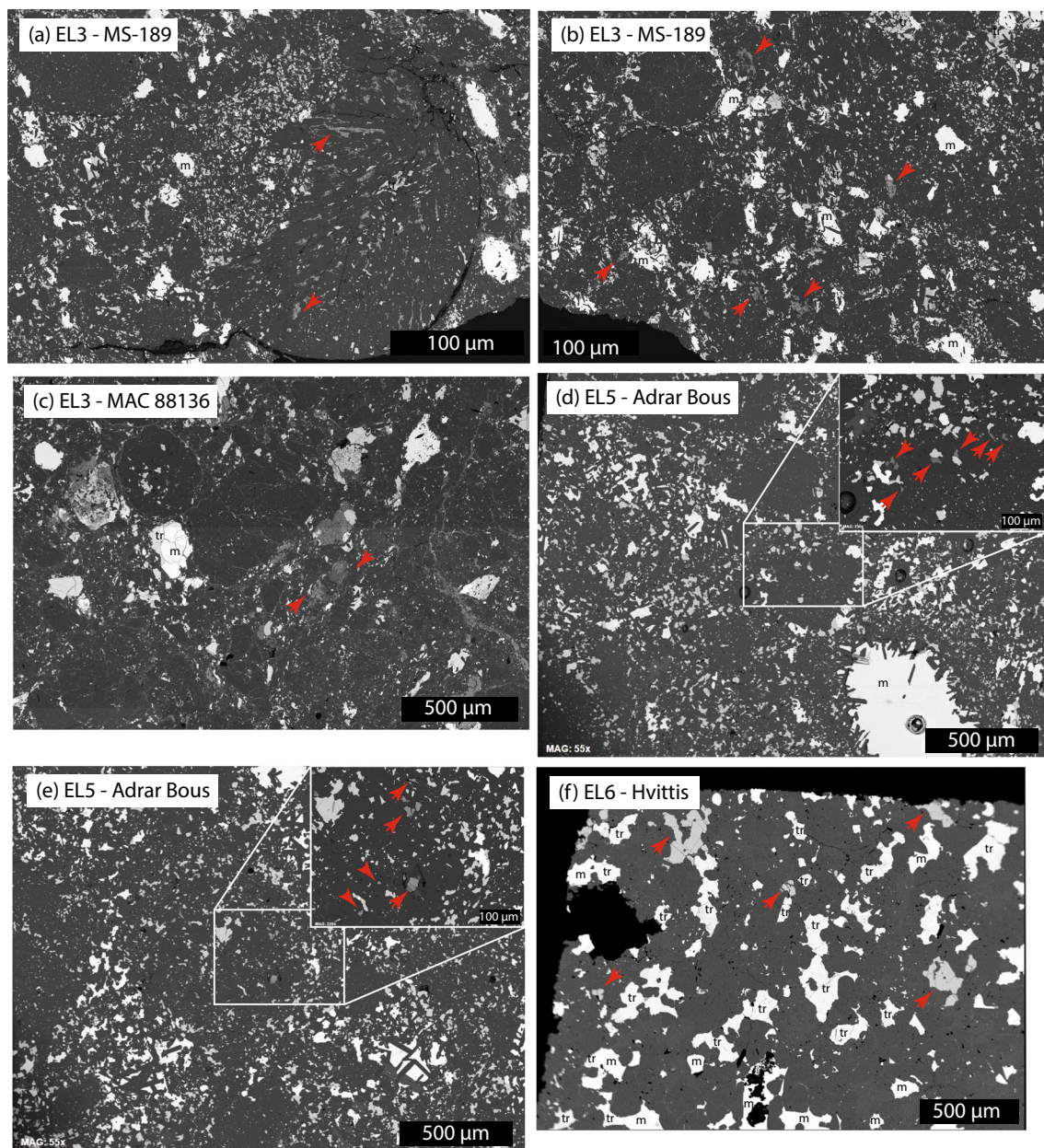


Fig. 3 Scanning electron images of some of the EL samples studied, illustrating the textural position of the oldhamite grains, indicated by the red arrows. Also indicated are the metal (m) and troilite (tr) grains

element (HREE) fractionation that appears to be step-wise around Eu.

In EL samples, all oldhamite types (EL3 to EL6) are characterized by upward convex CI-normalized REE patterns and negative Eu anomalies (Fig. 4b). In addition, oldhamites have constant compositions within each meteorite (a feature noted by Floss et al. 1990 in EL6), and REE abundances in all types have close values. CI-normalized La values range between 84 for MS-189

(EL3) and 143 for Adrar Bous (EL5), whereas $[Lu]_N$ values vary over a tighter range, from 67 in MS-189 and 84 in Adrar Bous. One EL3 (MAC 88136) appears exceptional with REE abundance values in CaS higher than the others, all $[REE]_N$ being larger than 150, except for Eu ($Eu/Eu^* = 0.57$). However, its overall pattern is not very different from the rest of the EL oldhamites. We do not exclude contamination by adjacent phases, resulting in normalization issue in this sample whose oldhamite

Table 2 Rare-earth element concentrations measured in CaS (in ppm) and Cl-normalized values

EH group	EH3				EH4		EH5			
	Sahara 97158 (28)		Caleta el Cobre (3)		Abee (8)		St-Mark's (8)		Oudiyat Sbaa (14)	
Concentration	ppm	stdev	ppm	stdev	ppm	stdev	ppm	stdev	ppm	stdev
La	9.31	2.46	10.97	0.62	18.85	4.11	17.26	2.17	15.22	0.96
Ce	17.05	5.45	20.78	3.68	49.38	7.16	42.33	6.26	39.36	2.91
Pr	1.88	0.73	2.63	0.73			6.31	1.03	5.83	0.38
Nd	7.75	3.10	10.99	3.39	38.18	4.44	32.60	3.77	30.40	2.82
Sm	2.69	1.14	4.20	1.06	12.68	1.73	10.85	1.76	10.09	0.76
Eu	3.48	0.49	3.76	0.48	3.08	0.62	4.11	0.71	3.76	0.44
Gd	1.98	0.95	3.42	1.28	15.81	2.00	13.95	1.59	12.81	1.42
Tb	0.33	0.17	0.60	0.22			2.55	0.34	2.46	0.39
Dy	2.21	1.14	3.98	1.40	17.33	1.47	17.06	2.01	16.91	1.62
Ho	0.46	0.23	0.86	0.28			3.81	0.44	3.64	0.26
Er	1.37	0.68	2.68	0.83	10.84	1.65	10.46	1.26	11.04	1.00
Tm	0.22	0.11	0.40	0.16			1.56	0.19	1.61	0.18
Yb	6.81	2.40	7.39	0.94	10.39	1.04	11.10	1.90	10.88	1.15
Lu	0.21	0.09	0.49	0.14	1.55	0.26	1.67	0.31	1.68	0.21
Cl-normalized concentration		stdev		stdev		stdev		stdev		stdev
La	39.62	10.48	46.68	2.64	80.22	17.47	73.46	9.22	64.76	4.07
Ce	28.42	9.08	34.63	6.13	82.30	11.93	70.56	10.43	65.60	4.86
Pr	20.61	7.99	28.94	7.98			69.29	11.34	64.09	4.14
Nd	16.70	6.68	23.69	7.30	82.28	9.56	70.26	8.12	65.51	6.09
Sm	17.56	7.47	27.43	6.93	82.87	11.28	70.88	11.48	65.92	4.97
Eu	59.32	8.33	64.11	8.11	52.50	10.64	70.12	12.07	64.14	7.52
Gd	9.61	4.62	16.59	6.20	76.75	9.72	67.71	7.73	62.16	6.89
Tb	8.74	4.59	15.91	5.99			67.91	9.09	65.47	10.47
Dy	8.69	4.48	15.67	5.50	68.23	5.80	67.16	7.92	66.59	6.38
Ho	8.08	4.09	15.13	4.90			67.23	7.73	64.38	4.56
Er	8.23	4.09	16.16	5.02	65.31	9.96	63.01	7.61	66.50	6.03
Tm	8.33	4.33	15.24	5.95			59.54	7.38	61.26	7.01
Yb	40.54	14.28	43.97	5.59	61.85	6.21	66.09	11.31	64.78	6.82
Lu	8.39	3.84	19.96	5.73	62.81	10.47	68.00	12.57	68.39	8.34
EL group	EL3				EL4/5				EL5	
	MAC 88136 (4)		MS 17 (12)		MS 189 (27)		MS 196 (18)		Adrar Bous (11)	
Concentration	ppm	stdev	ppm	stdev	ppm	stdev	ppm	stdev	ppm	stdev
La	34.06	8.59	20.96	1.49	19.78	2.24	21.96	0.78	33.67	3.09
Ce	97.36	14.04	54.95	3.49	50.23	4.77	57.88	3.20	82.57	8.65
Pr	15.50	3.03	8.00	0.48	7.59	1.42	8.90	0.88	12.19	1.39
Nd	80.20	12.96	42.46	2.38	38.94	9.79	44.27	2.27	62.73	6.33
Sm	26.08	3.19	14.59	0.68	12.83	1.96	13.53	1.66	19.70	2.09
Eu	5.57	1.43	2.60	0.17	2.37	0.40	2.33	0.43	2.79	0.25
Gd	33.57	3.35	19.91	1.07	15.74	1.98	19.99	2.27	25.78	1.99
Tb	6.38	0.92	3.56	0.18	2.98	0.43	3.35	0.25	4.57	0.35
Dy	43.58	4.83	25.14	1.47	19.59	2.40	23.76	1.14	29.69	2.25
Ho	8.94	1.46	5.33	0.26	4.44	0.77	5.12	0.43	6.30	0.45
Er	28.01	3.02	15.73	0.90	12.63	1.61	15.02	1.21	16.93	1.34
Tm	4.17	0.63	2.24	0.12	1.75	0.23	2.05	0.28	2.35	0.21
Yb	29.52	1.86	15.37	0.73	13.39	2.24	12.84	1.84	15.78	1.24

Table 2 (continued)

EL group	EL3						EL4/5		EL5	
	MAC 88136 (4)		MS 17 (12)		MS 189 (27)		MS 196 (18)		Adrar Bous (11)	
Concentration	ppm	stdev	ppm	stdev	ppm	stdev	ppm	stdev	ppm	stdev
Lu	3.77	0.66	2.08	0.11	1.65	0.21	1.99	0.41	2.05	0.15
Cl-normalized concentration		stdev		stdev		stdev		stdev		stdev
La	144.93	36.54	89.20	6.36	84.19	9.53	93.56	3.32	143.28	13.14
Ce	162.26	23.40	91.58	5.82	83.72	7.95	95.95	5.33	137.62	14.42
Pr	170.36	33.27	87.94	5.26	83.42	15.58	99.93	9.67	133.97	15.24
Nd	172.85	27.93	91.51	5.13	83.92	21.10	97.86	4.89	135.20	13.63
Sm	170.42	20.83	95.35	4.47	83.83	12.82	91.96	10.87	128.73	13.68
Eu	95.09	24.33	44.31	2.93	40.48	6.77	41.62	7.35	47.68	4.24
Gd	162.94	16.27	96.63	5.21	76.40	9.63	101.68	11.02	125.17	9.66
Tb	170.00	24.50	94.93	4.80	79.35	11.34	92.21	6.59	121.87	9.27
Dy	171.56	19.02	98.97	5.80	77.14	9.46	97.91	4.49	116.89	8.86
Ho	157.99	25.84	94.15	4.65	78.47	13.66	92.10	7.52	111.25	7.98
Er	168.72	18.22	94.78	5.40	76.08	9.73	94.51	7.31	101.97	8.10
Tm	159.26	23.99	85.57	4.77	66.81	8.64	84.91	10.53	89.72	7.88
Yb	175.71	11.10	91.47	4.34	79.67	13.31	79.00	10.96	93.92	7.40
Lu	153.15	26.68	84.64	4.41	67.19	8.43	81.80	16.77	83.41	6.25
EL group	EL6									
	NWA 974 (14)		Atlanta (15)		Hvittis (8)					
Concentration	ppm	stdev	ppm	stdev	ppm	stdev				
La	26.70	1.93	22.84	1.07	22.56	1.05				
Ce	69.97	4.94	59.06	2.62	59.45	1.62				
Pr	10.46	0.67	8.99	0.42	9.31	0.44				
Nd	57.55	4.27	48.79	2.56	52.41	2.74				
Sm	18.59	1.11	15.76	0.78	17.02	0.88				
Eu	1.98	0.19	2.10	0.19	1.68	0.12				
Gd	25.39	2.74	21.90	0.98	23.98	1.36				
Tb	4.42	0.27	3.87	0.16	4.23	0.24				
Dy	29.51	2.52	25.46	1.27	28.08	2.12				
Ho	6.22	0.50	5.55	0.34	6.04	0.47				
Er	16.53	1.52	14.86	0.80	16.00	0.92				
Tm	2.26	0.22	2.06	0.14	2.18	0.14				
Yb	14.56	1.26	13.04	0.90	14.10	0.94				
Lu	1.95	0.28	1.82	0.11	1.90	0.14				
Cl-normalized concentration		stdev		stdev		stdev				
La	113.60	8.23	97.18	4.53	96.02	4.45				
Ce	116.62	8.23	98.43	4.36	99.08	2.69				
Pr	114.91	7.32	98.77	4.64	102.31	4.87				
Nd	124.03	9.21	105.15	5.52	112.94	5.91				
Sm	121.53	7.28	103.00	5.10	111.21	5.76				
Eu	33.78	3.22	35.76	3.26	28.67	1.98				
Gd	123.23	13.31	106.29	4.78	116.39	6.61				
Tb	117.78	7.21	103.09	4.32	112.70	6.37				
Dy	116.18	9.90	100.22	5.00	110.56	8.34				
Ho	109.83	8.83	98.02	6.07	106.74	8.24				
Er	99.56	9.15	89.51	4.83	96.39	5.53				
Tm	86.12	8.27	78.60	5.25	83.29	5.33				

Table 2 (continued)

EL group	EL6					
	NWA 974 (14)		Atlanta (15)		Hvittis (8)	
Yb	86.65	7.49	77.60	5.37	83.92	5.58
Lu	79.08	11.21	73.95	4.57	77.06	5.88

CI values were taken from Barrat et al. (2012)

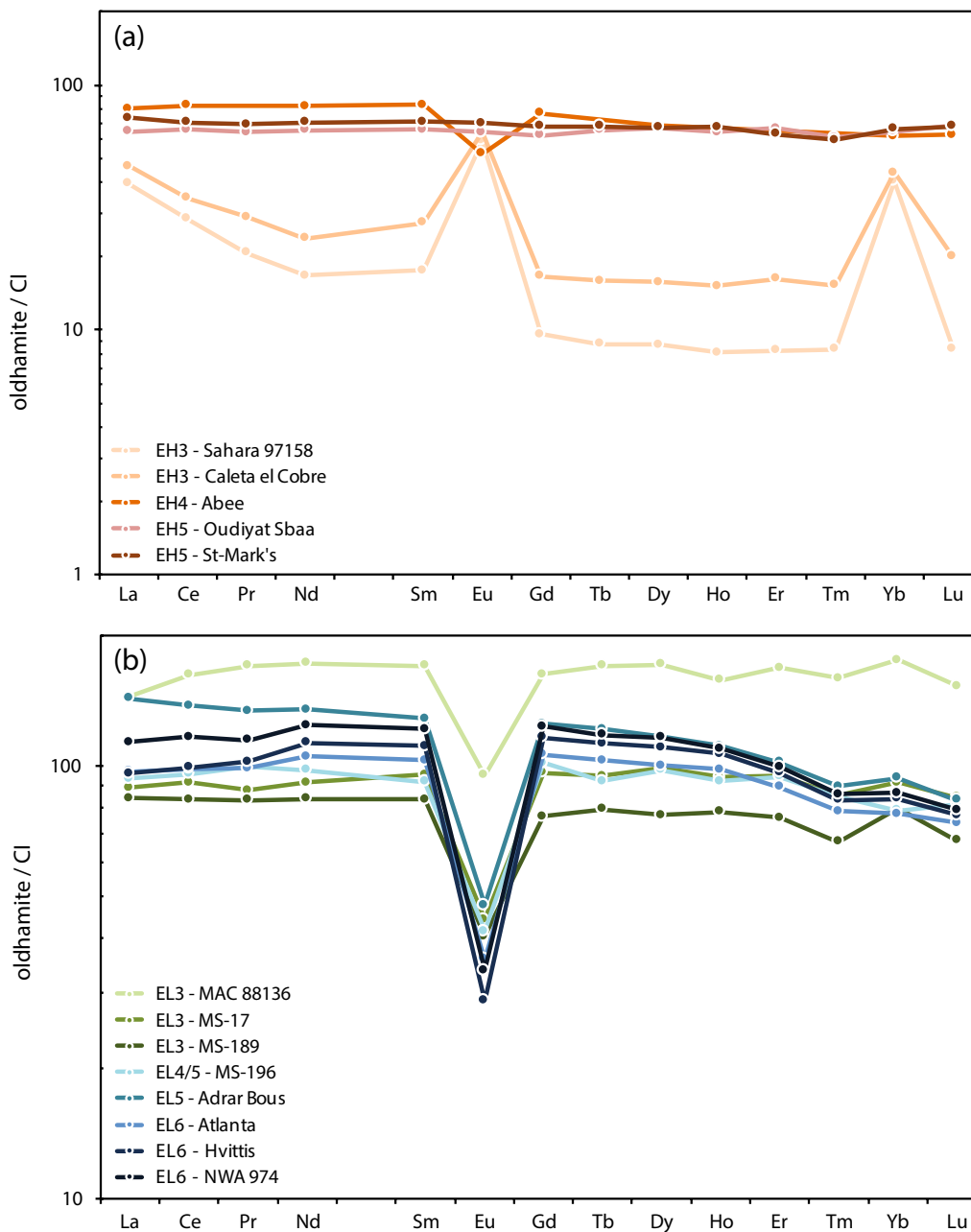


Fig. 4 CI-normalized REE abundances in oldhamites from EH chondrites (a) and EL chondrites (b). CI values are from Barrat et al. (2012)

grains are small and often altered. Concerning the Eu anomaly, it seems that Eu/Eu^* decreases from 0.57 in EL3 (MAC 88136) to 0.25 in EL6 (Hvittis). Our REE results are compatible with literature data on EL3 MAC 88136 and EL6 Jajh Deh Kot Lalu and Khairpur (Crozzaz and Lundberg 1995; Floss and Crozzaz 1993).

3.4 Rare-earth element concentrations in enstatites

Rare-earth element concentrations obtained in enstatites are illustrated in Fig. 5, as CI-normalized patterns. The measured concentrations are given in the Additional file 1. The dataset presented here is limited given the difficulty of obtaining reliable data. This limitation is due to low REE concentrations in most enstatite grains ($[\text{REE}]_N < 1$), which are small ($< 100 \mu\text{m}$) and often contain inclusions. Except in the case of equilibrated EL6, it is thus not clear whether the observed within-sample variations are accurate or caused by contamination from neighborhood phases. This also has consequences for data reduction because it raises uncertainties on the internal standard concentration used for normalization. In case the laser beam samples material that is not pure enstatite, the assumed internal standard concentration used for data reduction may be wrong. Those aspects have been previously discussed by Hsu and Crozzaz (1998) who distinguished three groups of enstatites according to their REE patterns. Group III enstatites are strongly depleted in the middle rare-earth elements (MREE) relative to HREE. LREE could not be measured because the concentrations are too low. These patterns are compatible with equilibrium with a melt (Cartier et al. 2014). Enstatites from groups I and II have patterns that are flatter or slightly depleted in LREE relative to HREE and could have been influenced by non-equilibrium processes including melt-inclusion trapping or other processes, such as discussed by Jacquet et al. (2012, 2015).

In the case of EH3, ALHA77295 enstatites have $[\text{REE}]_N$ values ranging between slightly less than 0.1 and 1 times CI. Some grains show HREE/LREE fractionation, but many have flat $[\text{REE}]_N$ patterns. Several grains display a negative Yb anomaly, whereas none is observed for Eu. In Sahara 97096 (EH3), enstatite CI-normalized REE patterns scatter over a wider range, from less than 0.1 to 4 times CI. The patterns are overall flat and, if not systematic, negative Eu and Yb anomalies appear to be common. In some cases, HREE/LREE fractionation is present. In EH of higher metamorphic grades (Abee, St. Mark's, and Oudiyat Sbaa), REE abundances in enstatites were below detection limits and no data could be obtained.

For EL chondrites, we obtained enstatite REE concentrations for at least one sample in metamorphic grades 3, 5, and 6. In MAC 88136 (EL3), CI-normalized REE concentration range between less than 0.02 to about 2.6.

Overall, enstatites in MAC 88136 have REE patterns that are close to those found in Sahara 97096 (EH3). The patterns in MAC 88136 are slightly fractionated ($[\text{La}/\text{Lu}]_N$ in MAC 88136 less than 1 in most cases) and a negative Yb anomaly is present. Some patterns also have a negative Eu anomaly, which is accompanied by a negative Sm anomaly in most cases. When shifting to EL chondrites of higher metamorphic grades, REE element patterns in enstatite display two changes: (1) a clustering of the concentration values, which is particularly clear for the HREE, with $[\text{Lu}]_N$ of about 1.1; (2) a HREE/LREE fractionation, reaching a value of $[\text{Lu}/\text{La}]_N$ of 348 for the most extreme case (in NWA 974). This evolution is accompanied by enstatite grain coarsening from Adrar Bous (EL5) to NWA 974 (EL6). The latter case illustrates the potential analytical biases. For HREE, the standard deviation is very small, reflecting the smaller potential for contamination by material adjacent to enstatite grains. Toward MREE and LREE, the effect of contamination increases as the concentrations decrease, resulting in a larger dispersion of the measured concentrations, and is particularly critical for Eu. If we consider that the most fractionated pattern represents the 'best' values, we can document a negative Eu anomaly ($\text{Eu}/\text{Eu}^* = 0.067$). We also note that the contaminant phase is enriched in LREE and has a positive Eu anomaly, suggesting that plagioclase could be a good candidate. We did not attempt to identify nearby plagioclase, because we focused on oldhamite features.

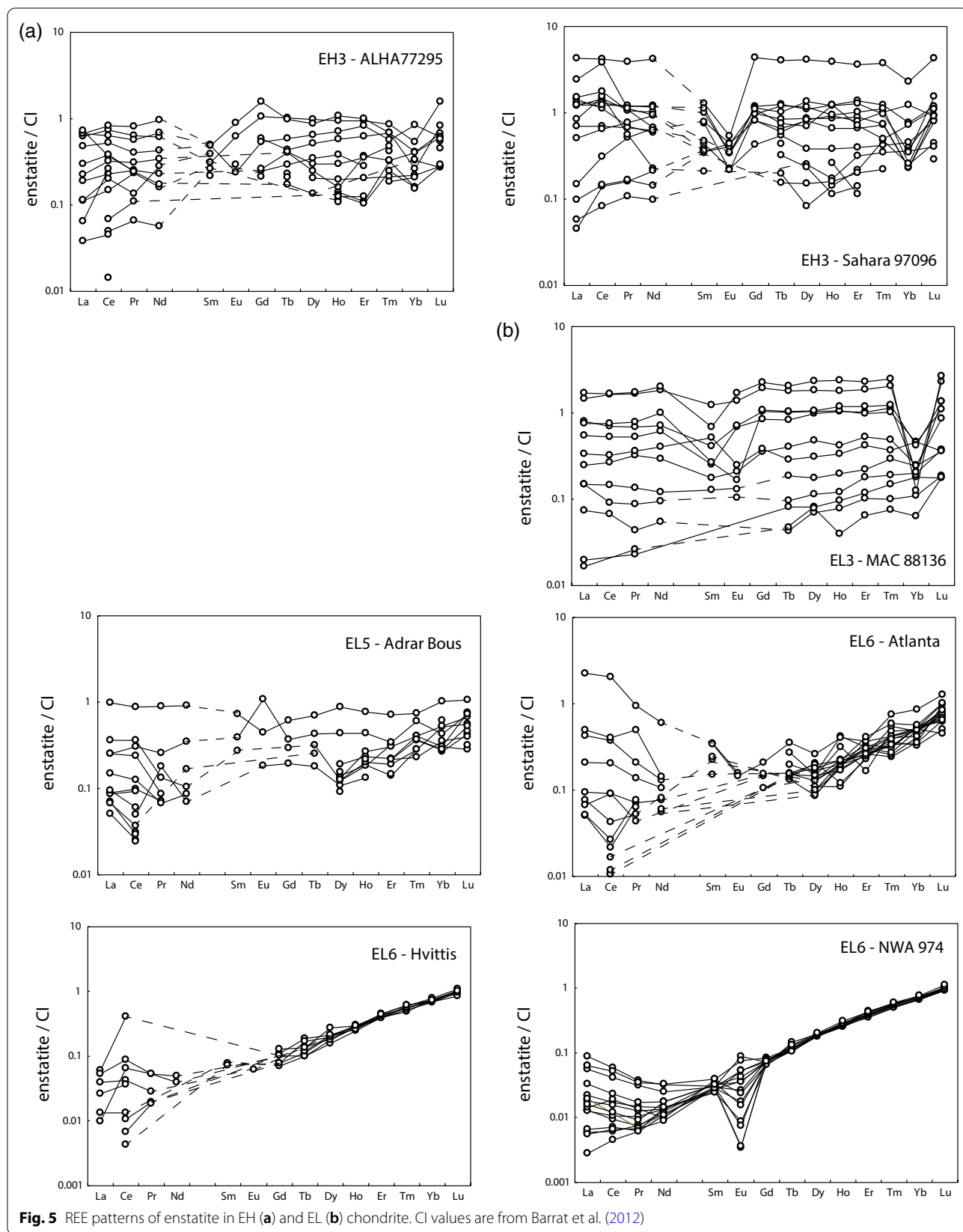
Our results on enstatite REE patterns compare well with those of Hsu and Crozzaz (1998) and Gannoun et al. (2011). In unequilibrated enstatite chondrites, we observe high variability for all REE concentrations, which may reflect contaminations or non-equilibrium processes. Highly fractionated patterns (accompanied by a negative Eu anomaly) found in EL6 enstatite may reflect equilibration with melt, as suggested by Hsu and Crozzaz (1998).

4 Discussion

We now discuss possible origins for the 3 major types of oldhamite REE patterns found in the present study: (1) in primitive EH chondrites; (2) in equilibrated EH chondrites; (3) in EL chondrites, all petrologic types being similar. Finally, we attempt to reconcile in situ mineral analysis, leaching, and bulk REE data.

4.1 Oldhamite in EH3 as condensates of residual gas?

In the present investigation, all oldhamites analyzed in EH3 (28 in Sahara 97158 and 3 in Caleta el Cobre 025) display the same REE patterns (Fig. 4), that labelled C-D in Crozzaz and Lundberg (1995) and Gannoun et al. (2011). None of the other pattern types (A, B, E) has been



found within the 28 oldhamite analyses in Sahara 97158. Caleta el Cobre 025 contains only a few oldhamite grains suitable for analysis. Gannoun et al. (2011) found that pattern type C-D was the most abundant in EH3, representing 56 and 97% of the analyses in ALHA77295 and Sahara 97072, respectively. It is possible that we missed the rare grains displaying other types given their scarcity, taking into account that Sahara 97158 and 97072 are paired (Grossman 1998).

The salient feature of EH3 oldhamites (this study and Gannoun et al. 2011) is their marked positive Eu and Yb anomalies combined with their moderate positive Sm anomaly and downward convex overall REE patterns. The positive Eu and Yb anomalies are compatible with experimental oldhamite/melt REE partition coefficients (Ingrao et al. 2019). The presence of Eu^{2+} and Yb^{2+} in the reduced environment of enstatite chondrite formation has been confirmed by X-ray Absorption Near Edge Structure (XANES) measurements of the experimental products obtained in reduced environments similar to that of enstatite chondrite parent body formation (Ingrao et al. 2019). The valence state for Eu has not been measured but results from Ingrao et al. (2019) suggest that all the Eu is present in its 2+ valence state whereas the 2+/3+ ratio decreases from Yb to Sm. However, the experimentally determined partition coefficient values are between 0.1 and 1, which cannot explain the high REE concentrations by a single stage of oldhamite/silicate melt equilibration. In addition, oldhamite/silicate melt equilibrium is not compatible with the shape (convexity) of the REE patterns found in EH3 oldhamite.

Another possibility is that the positive Eu and Yb anomalies are inherited from a condensation process. Gannoun et al. (2011) have dismissed CaS in primitive EH as early condensates because the positive Eu and Yb anomalies are not compatible with the REE patterns that are modeled for condensation sequence under reduced conditions (Lodders and Fegley 1993). Europium and Yb are the two REE characterized by the lowest condensation temperatures so they should be depleted in an early condensate, in a manner identical to that identified in CAIs (e.g., El Goresy et al. 2002) or in the mesostasis of chondrules of ordinary chondrites (Pack et al. 2004). Rare-earth element patterns measured in EH3 oldhamites may indicate that the material that is now present in

this phase may originate from a fraction that remained in the gas after an earlier condensation event, in a manner described for fine-grained CAI in carbonaceous chondrites (Davis et al. 2018).

We have calculated a first-order model adapted from that used by Davis et al. (2018) and by using their spreadsheet with thermodynamic data relevant to low oxygen fugacity conditions. For our model, we considered that REE condense in CaS, which appears at high temperature in the condensation sequence, according to Lodders and Fegley (1993). We compiled available thermodynamic data for REE sulfides (Mills 1974; Pankratz et al. 1987; Barin 1995). We used the formation enthalpies and the entropy values to parameterize the Gibbs free energy for the formation of gaseous (REE monoxides) and condensed (REE sesquisulfides, except for Eu and Yb where monosulfides were also used) species. Contrary to Lodders and Fegley (1993) we considered REE sesquisulfides in the condensed phase, by generalizing the experimental observation using XANES of the presence of Ho^{3+} in CaS equilibrated at low oxygen fugacity (between 5.8 and 6.6 log unit below the Fe-FeO (IW) equilibrium, Ingrao et al. 2019). Because Ingrao et al. (2019) also identified Eu^{2+} and Yb^{2+} in their experiments, we considered these two species in the calculations. Finally, following Drake and Boynton (1988), we calculated the activity coefficients for the REE in oldhamite using the partition coefficient values of Ingrao et al. (2019). The obtained activity coefficients are given in Table 3.

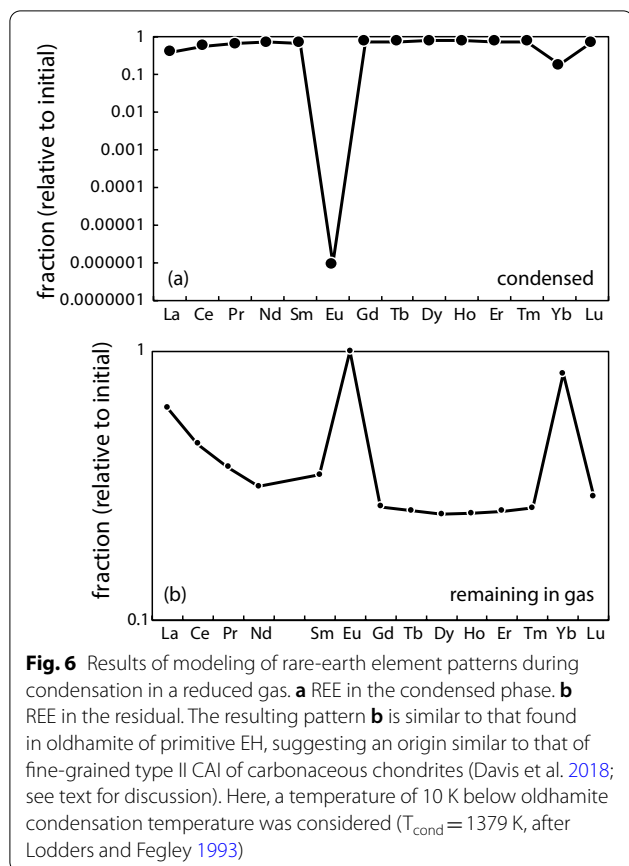
Our model predicts a first generation of CaS condensates, with upward convex pattern and negative Eu and Yb anomalies (Fig. 6). This shape is similar to some extent to that calculated by Lodders and Fegley (1993). Differences arise because we considered sesquisulfides and activity coefficients for the REE in solution in oldhamite. The results obtained for the REE fraction remaining in the gas are given in Fig. 6. Calculations have been done using a ΔT of 10 K ($T_{\text{condensation}}$ of oldhamite = 1379 K for $P_{\text{tot}} = 10^{-3}$ atm, after Lodders and Fegley 1993) so as to reproduce the values of the negative anomalies measured in Eu and Yb in EH3 oldhamites. It should be noted that the uncertainties are large because the thermodynamic database is in large part extrapolated or obtained by analogy with oxide energies of formation (see discussion in Mills 1974).

Table 3 Activity coefficients for REE in oldhamite

	La	Ce	Pr	Nd	Sm	Eu	Gd	Tb	Dy	Ho	Er	Tm	Yb	Lu
$\gamma(\text{REE}^{2+})$						1.49							3	
$\gamma(\text{REE}^{3+})$	1617	970	693	539	441	431 ^a	422	441	462	511	571	647	764 ^a	882

All coefficients apply to REE^{3+} , except for Eu^{2+} and Yb^{2+} , which have also been considered. Given the oxygen fugacity range, Ce^{4+} has not been considered here

^a For Eu^{3+} and Yb^{3+} , activity coefficients have been interpolated from other REE^{3+} values



Despite this limitation, it can be seen that the modeled REE pattern reflects the higher volatility of Eu and Yb, and Sm, to a lesser extent. Using the activity coefficient dataset gives the pattern a significant curvature and the resulting combination of curvature and anomalies is a pattern that is qualitatively similar to the observed EH3 oldhamite REE patterns. This mechanism that produces the oldhamite in primitive EH chondrites is therefore similar to what has been discussed for fine-grained (group II) CAIs in Allende CV chondrite by Davis et al. (2018), whose model considered the condensation of material remaining in the gas after hibonite condensation. Recently, Hu et al. (2021) have reconsidered the model of Davis et al. (2018) by taking into account REE stable isotope compositions. In particular, Hu et al. (2021) propose that group II CAIs result from evaporation followed by condensation. Because we are presently lacking REE stable isotope data on CaS, it is difficult to constrain the process of EH3 oldhamite formation better than proposed here. Whatever the detailed mechanism involved, it remains clear, however, that EH3 oldhamite cannot result from direct condensation from the nebula and that a two-stage process (at least) is necessary to explain REE abundance patterns.

4.2 Missing early oldhamite condensate in EH3 matrix

The postulated first generation of CaS condensates, which should be depleted in the most volatile REE and then characterized by negative Eu, Yb and Sm anomalies, has never been identified so far. One possibility is that this material is present in the matrix and that it is too fine grained for sampling with any current methods. Otherwise, it may be that this material has been lost or reprocessed during planetary body formation. El Goresy et al. (2017) suggested that small oldhamite grains associated with sinoite in EL3 MS-17 and MS-177 of the Almahatta Sitta breccia could be formed by condensation. However, the grains were too small (few μm) and a comparison with the expected EH signature is not possible, unfortunately. The possibility for an early condensate present in the matrix is now addressed.

Table 4 summarizes available REE data on EH3 chondrite phases. Here, we focus on Sahara 97158, which, together with its paired Sahara 97072 and Sahara 97096 (Grossman 1998) represents a well-documented material with REE measured on bulk sample, from leaching experiments, as well as in-situ measurements on oldhamites, enstatites and niningerites. Whole rock REE abundances were averaged from Gannoun et al. (2011) and Barrat et al. (2014). In situ analyses for oldhamite and enstatite are from this study and niningerite data are from Gannoun et al. (2011). Using the mineral proportions defined by Gannoun et al. (2011, 60% enstatite, 1.1% oldhamite, 1% niningerite), we have calculated a REE budget of Sahara 97158. The results show a deficit for most REE, which has been labelled 'missing' in Table 4. The missing component can represent as much as half the element budget for Ho and Er. For Eu and Yb, the deficit is lower, with values of 5.9 and 18.1%, respectively. Therefore, the missing component has negative Eu and Yb anomalies (Fig. 7). This component bears similarities with some chondrule mesostasis analyzed in the EH3 Sahara 97096 by Jacquet et al. (2015).

Uncertainties in the mass balance exist due to uncertainties in mineral proportions and REE concentrations in individual minerals. Nevertheless, there is little doubt that a significant part of the REE budget is missed when reconstructing the whole rock from individual mineral analyses. We suggest that the missing component is present in the matrix. The REE pattern of the missing component is shown in Fig. 7, together with those of the whole rock, the individual minerals, and the budget based on mineral analyses. In Fig. 7, we consider that the missing component is carried by 1% of the whole rock, as the matrix may represent between 5 and 12% of the bulk EC (Rubin et al. 2009b). Changing the proportion of the missing component would

Table 4 Mass balance and EH3 reconstruction (1.1% oldhamite; 1% niningerite; 60% enstatite)

ppm	Sahara 97158	Oldh	Enst	Nining. ^c	Budget	Missing ^d	Missing
Fraction ^a	WR ^b	0.011	0.60	0.01			% ^e
La	0.227	9.31	0.177	0.075	0.21	0.017	7.6
Ce	0.571	17.05	0.520	0.087	0.50	0.070	12.3
Pr	0.088	1.88	0.065	0.021	0.06	0.028	32.1
Nd	0.434	7.75	0.301	0.070	0.27	0.168	38.6
Sm	0.136	2.69	0.086	0.049	0.08	0.054	40.0
Eu	0.054	3.48	0.020	0.022	0.05	0.003	5.9
Gd	0.189	1.98	0.136	0.016	0.10	0.086	45.3
Tb	0.034	0.33	0.025	0.001	0.02	0.016	45.8
Dy	0.238	2.21	0.167	0.026	0.12	0.113	47.5
Ho	0.054	0.46	0.036	0.012	0.03	0.027	50.2
Er	0.159	1.37	0.103	0.046	0.08	0.081	51.2
Tm	0.024 ^f	0.22	0.018	0.012 ^f	0.01	0.011	44.5
Yb	0.154	6.81	0.080	0.340	0.13	0.028	18.1
Lu	0.025	0.21	0.021	0.020	0.02	0.010	38.8
CI-norm	Sahara 97158	Oldh	Enst	Nining	Budget	Missing ^d	
La	0.964	39.62	0.753	0.320	0.89	7.317	
Ce	0.951	28.42	0.866	0.145	0.83	11.728	
Pr	0.966	20.61	0.711	0.235	0.66	31.031	
Nd	0.936	16.70	0.649	0.152	0.57	36.129	
Sm	0.889	17.56	0.561	0.323	0.53	35.595	
Eu	0.915	59.32	0.342	0.377	0.86	5.359	
Gd	0.918	9.61	0.660	0.077	0.50	41.578	
Tb	0.914	8.74	0.665	0.039	0.50	41.833	
Dy	0.937	8.69	0.658	0.103	0.49	44.524	
Ho	0.946	8.08	0.634	0.209	0.47	47.432	
Er	0.956	8.23	0.622	0.276	0.47	48.933	
Tm	0.932 ^f	8.33	0.701	0.457 ^f	0.52	41.508	
Yb	0.917	40.54	0.475	2.022	0.75	16.557	
Lu	1.013	8.39	0.866	0.817	0.62	39.315	

^a Mineral fractions were adapted from Gannoun et al. (2011)

^b WR is the average of whole rock analysis given by Gannoun et al. (2011) and Barrat et al. (2014)

^c Ningerite data from Gannoun et al. (2011)

^d The missing component was estimated by subtracting the contributions of the phases from the whole rock (WR) REE content

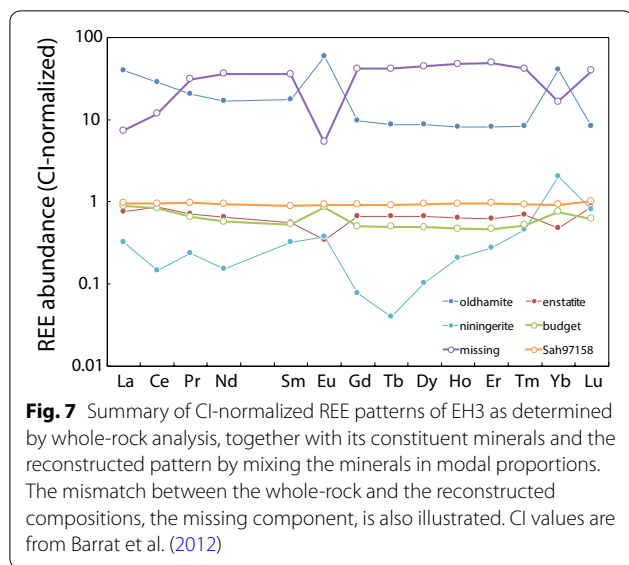
^e % represents the REE in the missing component relative to the WR composition

^f Tm in WR was not measured in Barrat et al. (2014), and Tm in niningerite was not analyzed by Gannoun et al. (2011). For mass balance purposes, Tm was interpolated using reported Er and Lu values

only shift its REE pattern, without altering its main features, that is, the negative Eu and Yb anomalies.

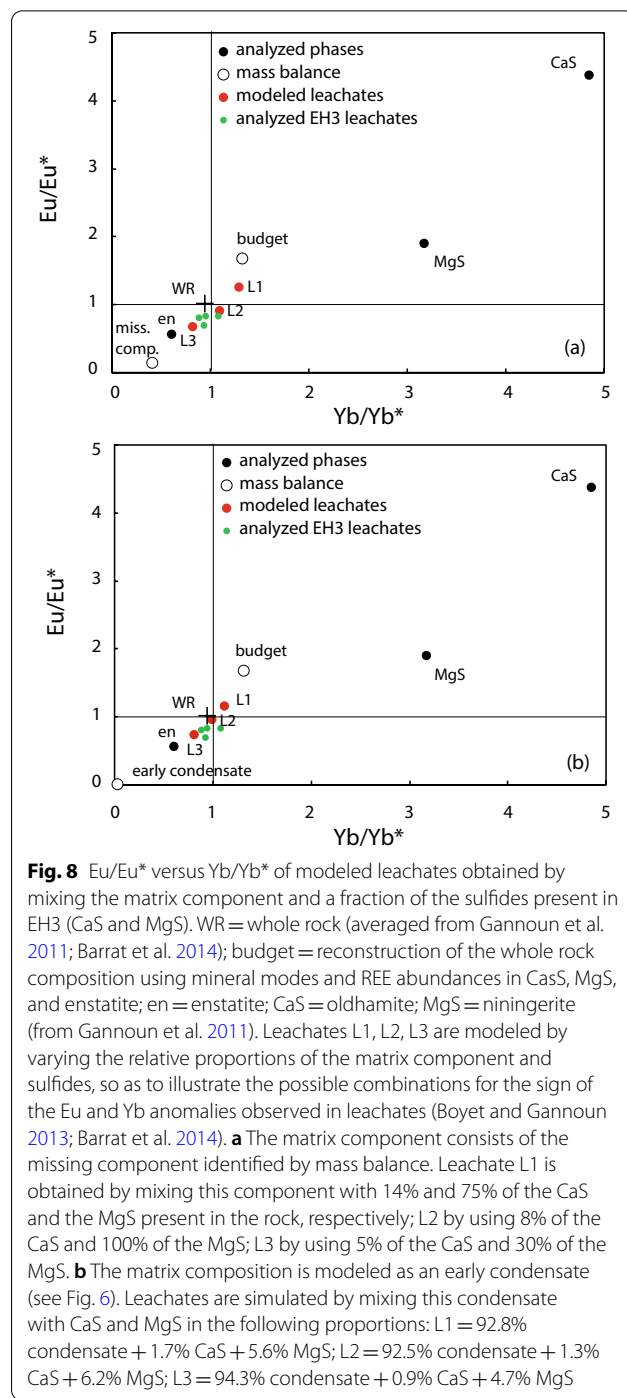
Stepwise dissolution and leaching, as performed by Boyet and Gannoun (2013) and Barrat et al. (2014), can be a way to access the information carried by the EH matrix that cannot be documented by in-situ analysis. Usually, the leachates of EH3 obtained with the weakest acid solutions are interpreted as representing the sulfide (CaS, MgS) contribution whereas the residual fraction should carry the silicate (enstatite) signature. It

is striking, however, that the leachates of EH3 obtained with the weakest acid solutions yield CI-normalized patterns with a slight positive Yb anomaly and only a slight negative Eu anomaly, which is different from those found in single CaS grains (by in situ analysis) that have strong positive anomalies for both Eu and Yb. These results confirm that the missing component is a sulfide phase present in the fine-grained matrix because it is dissolved in the first leaching using 0.5 M acetic acid (Boyet and Gannoun 2013).



We have attempted to reconcile in situ and leaching data by considering the contribution of a component present in the matrix, such as the missing component discussed above. We have modeled REE CI-normalized pattern of a mixture consisting of the missing component and a fraction of the CaS and the MgS present in the chondrite. The result is displayed in Fig. 8. Given the overall uncertainties in phase proportions, REE abundances in minerals (particularly LREE in enstatite and MgS), it is worth noting that the resulting combination possesses negative and positive anomalies for Eu and Yb, respectively, as observed in EH3 leachates. The overall LREE to HREE fractionation of the modeled missing component differs slightly from that observed in the leachates, but the LREE budget relies heavily on enstatite compositions, which bear significant uncertainty. Therefore, we consider that our model serves to illustrate that in situ and leaching data can be reconciled.

Mixing single grains and matrix contributions can be further explored by modeling the matrix using a condensation sequence. As mentioned above, CaS of primitive chondrites can be modeled as condensing from a reduced residual gas (Ebel 2006). Given the Eu and Yb positive anomalies observed in CaS, the first condensate has negative anomalies for both elements, and therefore resembles the missing component discussed above, on the basis of mass balance calculations. We have mixed this early condensate with fractions of CaS and MgS, in a manner similar to that used above, for the missing component. Using appropriate proportions of both sulfides, it is possible to reproduce the expected anomalies for Eu and Yb, as illustrated in Fig. 8. Here,



as elsewhere, the major uncertainties arise from the thermodynamic data used for condensation modeling.

Both models presented have uncertainties and large degrees of freedom, but it is worth noting that both the missing component and the calculated early condensate have negative Eu and Yb anomalies. We suggest that this contribution that is not detectable by in situ analysis of

single grains can be documented by step-leaching methods, although its contribution is partly blurred by mixing with other sulfides.

4.3 Oldhamite of EH5 as reflecting sulfide/matrix equilibration?

Oldhamites from the two EH5 studied (St. Mark's and Oudiyat Sbaa) have flat REE patterns. Oldhamites from Abee (EH4/IMB) are also flat but, in addition, have a slight negative Eu anomaly. Here, we only discuss the EH5 data, and ignore Abee, which is an impact melt breccia that has experienced some degree of melting. Abee is strongly heterogeneous as observed in the REE pattern obtained from bulk rock measurements. The Abee rare-earth element pattern obtained by Boyet et al (2018) has a negative Eu anomaly ($\text{Eu}/\text{Eu}^* = 0.83$) whereas the pattern is flat in the piece analyzed by Barrat et al (2014). Therefore, Abee appears to have been affected by secondary processes (i.e., impact metamorphism and/or melting) and is not a good candidate to discuss parent-body processes.

The flat character of REE patterns in EH5 oldhamites can be interpreted as representing unfractionated REE condensation. It can also be interpreted as reflecting inter-grain redistribution during textural maturation associated with metamorphic evolution incomplete in EH3 and nearly complete in EH5 on their parent body. Unfractionated condensation could be caused by disequilibrium processes during condensation, but detailed mechanisms of this process are difficult to decipher (e.g., Jacquet and Marrocchi 2017). However, if we assume a genetic link between EH3 and EH5 oldhamites, it is necessary to consider that EH5 oldhamites have gained a significant fraction of all the REE but the most volatile ones (Eu and Yb), which are at the same level of concentration in EH3 and EH5. In the present state of our knowledge, the only mechanism possible would involve the contribution of a complementary reservoir present in the matrix of EH3, such as the missing part discussed above.

4.4 Oldhamite of EL chondrites as a record of a melting event?

The main characteristics of the REE patterns of oldhamite from EL chondrites are (1) that they bear no resemblance to those found in all EH types, (2) that they are all similar, with minor differences between types, and (3) that they are similar to those found in aubrites, that is enstatite achondrites (Floss and Crozaz 1993; Lodders et al. 1993; Wheelock et al. 1994).

From their observation of euhedral enstatite crystals growing on chondrule relicts and metal globules, Rubin and Scott (1997) argued for melting in Abee (EH4), which is an impact melt breccia. The oldhamite REE pattern

measured in Abee is more similar to those defined for the EL groups (Fig. 4). Later on, Rubin et al. (2009a) extended this observation to EL, which they noticed all presented evidence for melting, except for one. EL chondrites from type 6 are all characterized by depletion in LREE and are also depleted in Ca relative to EH samples. These features, first described by Rubin et al. (2009a), have been confirmed by Barrat et al. (2014) who also noted depletions in Nb and Eu and positive Y anomalies in EL6 samples and impact melt samples [e.g., Galim (b), LAP 02225, Barrat et al. (2014)]. Bulk trace element concentrations of EL6 clearly suggest that all samples from this subgroup have been affected by a melting event.

That CaS of all EL chondrite subgroups may have equilibrated with silicate melt is strongly substantiated by the REE pattern with its upward convex shape. Recently, Ingrao et al. (2019) reported a complete dataset for REE partitioning between oldhamite and silicate melt. The influence of radius size on REE behavior is a strong indication that crystal-melt equilibrium may be at work. A major difference between REE abundance in CaS of EL chondrites and partition coefficient values concerns the Eu and Yb anomalies. In the experiments, both elements have a positive anomaly, whereas in the CaS of EL, only Eu has a strong negative anomaly. One possible explanation for the low concentrations of Eu and Yb is the loss of a Fe and S-dominated vapor phase. Compared to EH, EL are depleted in iron and sulfur and available partition coefficients of REE between molten FeS and molten silicate (Lodders 1996; Ingrao et al. 2019) show that both Eu and Yb are preferentially incorporated in FeS, relative to other REE. In addition, Eu and Yb are the most volatile REE. It is therefore possible that melting was accompanied by partial vaporization, resulting in Eu and Yb loss and yielding the presently observed REE patterns in oldhamites of EL chondrites. Although this conclusion is at odds with the detailed analysis of El Goresy et al. (2017) on MS-17 and MS-177, we note that El Goresy et al. (1995) report on the preservation of carbon and nitrogen isotopic heterogeneities in the primitive achondrite Acapulco, which experienced partial melting. Moreover, we have no information on the timing because no data is available, but the melting event likely occurred very early before the accretion of the final parent body.

Whole rock data on EL chondrites often show depletion in Eu and/or Yb (Barrat et al. 2014). Recently, on the basis of metal and sulfide analysis, Horstmann et al. (2014) and Weyrauch et al. (2018) proposed that a previous parent body of enstatite chondrite affinity underwent melting and was dismantled, some or all of its fragments being later assembled to form the EL parent body. More recently, Kimura et al. (2021) proposed that MS-177, an EL3, underwent a high-temperature subsolidus event and

suggested that other E3 also underwent heating events. Moreover, Rindlisbacher et al. (2021) suggested that the metal-rich nodules found in a thin section of NWA 8785, which is classified as an EL3, recorded melting and evolved separately before being accreted on their parent body. Here, we suggest that all EL chondrites went through a high-temperature stage that involved some degree of melting and vaporization, whose effects are now recorded in EL oldhamite REE patterns.

There is agreement between leaching experiments on EL3 (Barrat et al. 2014) and REE patterns obtained from in situ single CaS grain analysis. They both show upward convex patterns with a negative Eu anomaly. This is markedly different from findings on EH3, as discussed above. The similarity between leaching and grain analyses in EL3 indicates that the contribution of the EL matrix to the REE budget (if any) is not different from that of the single grains. The high temperature (melting) stage discussed above to explain similar oldhamite patterns for all EL types may have contributed to matrix/grain equilibration as well.

5 Conclusions

The detailed analysis of REE in oldhamite from most known types of enstatite chondrites by laser ablation ICP-MS documents a striking contrast between EH and EL. Three major types of oldhamite REE patterns were distinguished. The first type, with marked positive Eu and Yb anomalies, is characteristic of unequilibrated EH chondrites (EH3). It may correspond to the condensation of a residual gas, following a two-stage process similar to that invoked by Davis et al. (2018) for fine-grained, type II CAIs. Because the whole rock EH3 REE budget cannot be reproduced by mass balance using individual grain compositions, a complementary reservoir must be present, perhaps in the fine-grained matrix. This component cannot be characterized by in situ methods, but its composition may be approached by mass balance. Stepwise dissolution of unequilibrated EH can sample this reservoir but published data seem to indicate that its signal is mixed with that of sulfide grains. The matrix contribution may consist of an early-condensed (but not macroscopic) sulfide (CaS). If, alternatively, EH oldhamite resulted from evaporation followed by condensation following the model recently proposed by Hu et al. (2021) for group II CAIs, the evaporated fraction must have remained on EH3 parent body to satisfy chondritic abundances for EH3 bulk rock REE. The lack of data on REE stable isotope composition of CaS does not allow to conclude further at the present stage.

A second type of oldhamite is characterized by flat REE patterns. It is found in equilibrated EH5 chondrites only. We suggest that it is the result of textural maturation

and chemical equilibration between the large oldhamite grains and the matrix. This evolution is accompanied by no bulk loss of material, even for the most volatile REE, such as Eu and Yb.

The third type of oldhamite is found only in EL chondrites, whatever their metamorphic type. It is similar to pattern measured in oldhamites from aubrites. The EL REE patterns bear some characteristics indicative of oldhamite/melt equilibrium, although some expected features are lacking, such as the positive Eu and Yb anomalies documented in the experimental petrology literature. This paradox can be solved by considering that melting was accompanied by partial volatilization, wherein a fraction Eu and Yb were lost to a Fe and S-rich gaseous phase. Given the high temperatures required for melting, it is not excluded that EL oldhamites could also carry the signature of evaporation followed by condensation, in a manner discussed by Hu et al. (2021). Perhaps data on REE stable isotope compositions, when available, will further contribute to our understanding of the origin of EL oldhamites. It remains that interaction with melt is also attested by enstatite REE patterns, but this is visible only in EL5 and EL6, although it may also be hinted at in EL3.

A striking finding from our survey is that oldhamites from all EL chondrites, even the least equilibrated ones (EL3) carry a signature that can be attributed to high temperature modification, melting and volatilization. Here, one must admit that overall chondritic elemental abundances were not lost during the process. One possibility is that melting and partial evaporation took place on the EL parent body itself and that either the melting degree or the gravity field was low enough to prevent large-scale differentiation of the EL parent body. The present data do not allow to determine at which stage of the EL history the high-temperature event took place. It may be on the parent body or prior to parent-body formation. It cannot be excluded that several heating events happened. It seems clear, however, that all EL, including the most unequilibrated ones have been processed at some stage and that they do not represent primary nebular material.

Supplementary Information

The online version contains supplementary material available at <https://doi.org/10.1186/s40645-022-00471-w>.

Additional file 1. Major element concentrations analyzed in oldhamites by electron microprobe, together with detection limits.

Acknowledgements

This work would not have been possible without Ahmed El Goresy who introduced us to the world of exotic sulfides that form in reduced conditions. We started to study and measure REE in sulfides from unequilibrated EH only.

The first results obtained on EL samples led to many discussions and stormy debates. We would have liked Ahmed El Goresy to give us his opinion on this manuscript. We thank him warmly for having transmitted us his passion. This work benefitted from discussion with Jean-Alix Barrat and Bertrand Moine. Comments and suggestions by Alan Rubin and Denton Ebel, as well as by editor Makoto Kimura are gratefully acknowledged. Assistance by J.-L. Devidal on electron microprobe and laser-ablation ICP-MS analyses and by J.-M. Hénot and E. Voyer with the scanning electron microscope is acknowledged. We thank I. Chargros and B. Wasilewski for their help at an early stage of this project. We thank INSU-CNRS (Programme National de Planétologie) for financial support. This research was partly supported by the French Government Laboratory of Excellence initiative ANR-10-LABX-0006, the Région Auvergne, and the European Regional Development Fund. This project has received funding from the European Research Council (ERC) under the European Union's Horizon 2020 research and innovation program (Grant Agreement No. 682778—ISOREE). This is Laboratory of Excellence ClerVolc contribution N° 511.

Authors' contributions

The project was designed by TH and MB. All authors contributed to the data acquisition. TH wrote the manuscript with discussions with MB, PF, and CC. All authors read and approved the final manuscript.

Funding

This work was supported by Programme National de Planétologie of CNRS-INSU, by the French Government Laboratory of Excellence initiative ANR-10-LABX-0006, the Région Auvergne, and the European Regional Development Fund. This project has received funding from the European Research Council (ERC) under the European Union's Horizon 2020 research and innovation program (Grant Agreement No. 682778—ISOREE).

Availability of data and materials

All data discussed in this paper are provided in the main text and in the supplementary information files.

Declaration

Competing interests

The authors declare that they have no competing interest.

Author details

¹CNRS, IRD, OPGC, Laboratoire Magmas et Volcans, Université Clermont Auvergne, 63000 Clermont-Ferrand, France. ²CRPG, CNRS, Université de Lorraine, UMR 7358, 54501 Vandœuvre-les-Nancy, France.

Received: 26 August 2021 Accepted: 31 January 2022

Published online: 21 February 2022

References

- Anzures BA, Parman SW, Milliken RE, Namur O, Cartier C, Wang S (2020) Effect of sulfur speciation on chemical and physical properties of very reduced mercurian melts. *Geochim Cosmochim Acta* 286:1–18
- Barin I (1995) Thermochemical data of pure substances, 3rd edn, VCH editions, 1885 pages
- Barrat J-A, Zanda B, Moynier F, Bollinger C, Liorzou C, Bayon G (2012) Geochemistry of CI chondrites: major and trace elements, and Cu and Zn Isotopes. *Geochim Cosmochim Acta* 83:79–92
- Barrat J-A, Zanda B, Jambon A, Bollinger C (2014) The lithophile trace elements in enstatite chondrites. *Geochim Cosmochim Acta* 128:71–94
- Boyett M, Gannoun A (2013) Nucleosynthetic Nd isotope anomalies in primitive enstatite chondrites. *Geochim Cosmochim Acta* 121:652–666
- Boyett M, Bouvier A, Frossard P, Hammouda T, Garçon M, Gannoun A (2018) Enstatite chondrites EL3 as building blocks for the Earth: the debate over the ¹⁴⁶Sm-¹⁴²Nd systematics. *Earth Planet Sci Lett* 488:68–78
- Burkhardt C, Kleine T, Oberli F, Pack A, Bourdon B, Wieler R (2011) Molybdenum isotope anomalies in meteorites: constraints on solar nebula evolution and origin of the Earth. *Earth Planet Sci Lett* 312:390–400
- Buseck PR, Holdsworth EF (1972) Mineralogy and petrology of the Yilmia enstatite chondrite. *Meteoritics* 7:429–447
- Cartier C, Wood BJ (2019) The role of reducing conditions in building Mercury. *Elements* 15:39–45
- Cartier C, Hammouda T, Doucelance R, Boyet M, Devidal J-L, Moine B (2014) Experimental study of trace element partitioning between enstatite and melt in enstatite chondrites at low oxygen fugacities and 5 GPa. *Geochim Cosmochim Acta* 130:167–187
- Cartigny P, Boyd SR, Harris JW, Javoy M (1997) Nitrogen isotopes in peridotitic diamonds from Fuxian, China: the mantle signature. *Terra Nova* 9:175–179
- Clayton RN (1993) Oxygen isotopes in meteorites. *Ann Rev Earth Planet Sci* 21:115–149
- Crozaz G, Lundberg LL (1995) The origin of oldhamite in unequilibrated enstatite chondrites. *Geochim Cosmochim Acta* 59:3817–3831
- Dauphas N, Marty B, Reisberg L (2002) Inference on terrestrial genesis from molybdenum isotope systematics. *Geophys Res Lett* 29:1084
- Davis AM, Zhang J, Greber ND, Hua J, Tissot F, Dauphas N (2018) Titanium isotopes and rare earth patterns in CAIs: evidence for thermal processing and gas-dust decoupling in the protoplanetary disk. *Geochim Cosmochim Acta* 221:275–295
- Dickinson TM, McCoy TJ (1997) Experimental rare-earth-element partitioning in oldhamite: implications for the igneous origin of aubritic oldhamite. *Meteor Planet Sci* 32:395–412
- Drake MJ, Boynton WV (1988) Partitioning of rare earth elements between hibonite and melt and implications for nebular condensation of the rare earth elements. *Meteoritics* 23:75–80
- Ebel DS (2006) Condensation of rocky material in astrophysical environments. In: Lauretta DS, McSween Jr. HY (eds) *Meteorites and the early solar system II*. University of Arizona Press, Tucson, pp 253–277
- Ebel DS, Alexander CMOD (2011) Equilibrium condensation from chondritic porous IDP enriched vapor: implications for Mercury and enstatite chondrite origins. *Planet Space Sci* 59:1888–1894
- El Goresy A, Zinner E, Marti K (1995) Survival of isotopically heterogeneous graphite in a differentiated meteorite. *Nature* 373:496–499
- El Goresy A, Zinner E, Matsunami S, Palme H, Spettel B, Lin Y, Nazarov M (2002) Efremovka 101.1: a CAI with ultrarefractory REE patterns and enormous enrichments of Sc, Zr, and Y in fassaite and perovskite. *Geochim Cosmochim Acta* 66:1459–1491
- El Goresy A, Lin Y, Miyahara M, Gannoun A, Boyet M, Ohtani E, Gillet P, Trierloff M, Simionovici A, Feng L, Lemelle L (2017) Origin of EL3 chondrites: evidence for variable C/O ratios during their course of formation: a state of art scrutiny. *Meteor Planet Sci* 52:781–806
- Floss C, Crozaz G (1993) Heterogeneous REE patterns in oldhamite from aubrites: their nature and origin. *Geochim Cosmochim Acta* 57:4039–4057
- Floss C, Strait MM, Crozaz G (1990) Rare earth elements and the petrogenesis of aubrites. *Geochim Cosmochim Acta* 54:3553–3558
- Gagnon JE, Fryer BJ, Samson IM, Williams-Jones AE (2008) Quantitative analysis of silicate certified reference materials by LA-ICPMS with and without an internal standard. *J Anal Spectrom* 23:1529–1537
- Gannoun A, Boyet M, El Goresy A, Devouard B (2011) REE and actinide microdistribution in Sahara 97072 and ALHA77295 EH3 chondrites: a combined cosmochemical and petrologic investigation. *Geochim Cosmochim Acta* 75:3269–3289
- Grossman JN (1998) The meteoritical bulletin, No. 82, 1998 July. *Meteor Planet Sci* 33:A221–A239
- Hammouda T, Chantel J, Devidal J-L (2010) Apatite solubility in carbonatitic liquids and trace element partitioning between apatite and carbonate at high pressure. *Geochim Cosmochim Acta* 74:7220–7235
- Horstmann M, Humayun M, Bischoff A (2014) Clues to the origin of metal in Almahata Sitta EL and EH chondrites and implications for primitive E chondrite thermal histories. *Geochim Cosmochim Acta* 140:720–744
- Hsu W (1998) Geochemical and petrographic studies of oldhamite, diopside, and roedderite in enstatite meteorites. *Meteor Planet Sci* 33:291–301
- Hsu W, Crozaz G (1998) Mineral chemistry and the origin of enstatite in unequilibrated enstatite chondrite. *Geochim Cosmochim Acta* 62:1993–2004
- Hu JY, Dauphas N, Tissot FLH, Yokochi R, Ireland TJ, Zhang Z, Davis AM, Ciesla FJ, Grossman L, Charlier BLA, Roskosz M, Alp EE, Hu MY, Zhao J (2021) Heating events in the nascent solar system recorded by rare earth element isotopic fractionation in refractory inclusions. *Sci Adv* 7:eabc2962
- Ingrao NJ, Hammouda T, Boyet M, Gaborieau M, Moine BN, Vlastelic I, Bouhifd MA, Devidal J-L, Mathon O, Testemale D, Hazemann J-L, Proux O (2019) Rare earth element partitioning between sulphides and melt: evidence

- for Yb²⁺ and Sm²⁺ in EH chondrites. *Geochim Cosmochim Acta* 265:182–197
- Jacquet E, Marrocchi Y (2017) Chondrule heritage and thermal histories from trace element and oxygen isotope analyses of chondrules and amoeboid olivine aggregates. *Meteor Planet Sci* 52:2672–2694
- Jacquet E, Alard O, Gounelle M (2012) Chondrule trace element geochemistry at the mineral scale. *Meteor Planet Sci* 47:1695–1714
- Jacquet E, Alard O, Gounelle M (2015) The formation conditions of enstatite chondrites: insights from trace element geochemistry of olivine-bearing chondrules in Sahara 97096 (EH3). *Meteor Planet Sci* 50:1624–1642
- Javoy M (1995) The integral enstatite chondrite model of the earth. *Geophys Res Lett* 22:2219–2222
- Javoy M, Pineau F, Delorme H (1986) Carbon and nitrogen isotopes in the mantle. *Chem Geol* 57:41–62
- Javoy M, Kaminski E, Guyot F, Andrault D, Sanloup C, Moreira M, Labrosse S, Jambon A, Agrinier P, Davaille A, Jaupart C (2010) The chemical composition of the Earth: Enstatite chondrite model. *Earth Planet Sci Lett* 293:259–268
- Kallemeyn GW, Wasson JT (1986) Compositions of enstatite (EH3, EH4, 5 and EL6) chondrites: implications regarding their formation. *Geochim Cosmochim Acta* 50:2153–2164
- Keil K (1968) Mineralogical and chemical relationships among enstatite chondrites. *J Geophys Res* 73:6945–6976
- Keil K (1969) Titanium distribution in enstatite chondrites and achondrites, and its bearing on their origin. *Earth Planet Sci Lett* 7:243–248
- Kimura M, Weisberg MK, Takaki A, Imae N, Yamaguchi A (2021) An Almahata Sitta EL3 fragment: implications for the complex thermal history of enstatite chondrites. *Prog Earth Planet Sci* 8:55
- Krot AN, Keil K, Scott ERD, Goodrich CA, Weisberg MK (2014) Classification of meteorites and their genetic relationships. In Davis AM (ed) *Meteorites, comets and planets*, vol 1, treatise on geochemical second edition (eds. K.K. Turekian and H.D. Holland). Elsevier, Oxford
- Lin Y, El Goresy AE (2002) A comparative study of opaque phases in Qingzhen (EH3) and MacAlpine Hills 88136 (EL3): representatives of EH and EL parent bodies. *Meteor Planet Sci* 37:577–599
- Lodders K (2003) Solar system abundances and condensation temperatures of the elements. *Astrophys J* 591:1220–1247
- Lodders K (1996) An experimental and theoretical study of rare-earth-element partitioning between sulfides (FeS, CaS) and silicate and applications to enstatite achondrites. *Meteor Planet Sci* 31:749–766
- Lodders K, Fegley B Jr (1993) Lanthanide and actinide chemistry at high C/O ratios in the solar nebula. *Earth Planet Sci Lett* 117:125–145
- Lodders K, Palme H, Wlotzka F (1993) Trace elements in mineral separates of the Pena Blanca Spring aubrite: implications for the evolution of the aubrite parent body. *Meteoritics* 28:538–551
- Mills KC (1974) *Thermodynamic data for inorganic sulphides, selenides and tellurides*. Butterworth, London
- Miura YN, Hidaka H, Nishiizumi K, Kusakabe M (2007) Noble gas and oxygen isotope studies of aubrites: a clue to origin and histories. *Geochim Cosmochim Acta* 71:251–270
- Pack A, Shelley JMG, Palme H (2004) Chondrules with peculiar REE patterns: implications for solar nebular condensation at high C/O. *Science* 303:997–1000
- Pankratz LB, Mah AD, Watson SW (1987) *Thermodynamic properties of sulfides*. United States Department of the Interior, Bureau of Mines Bulletin 689, 427 pages
- Pearce NJG, Perkins WT, Westgate JA, Gorton MP, Jackson SE, Neal CR, Chenery SP (1997) A compilation of new and published major and trace element data for NIST SRM 610 and NIST SRM 612 glass reference materials. *Geostand Newslett* 21:115–144
- Piani L, Marrocchi Y, Libourel G, Tissandier L (2016) Magmatic sulfides in the porphyritic chondrules of EH enstatite chondrites. *Geochim Cosmochim Acta* 195:84–99
- Regelous M, Elliott T, Coath CD (2008) Nickel isotope heterogeneity in the early Solar System. *Earth Planet Sci Lett* 272:330–338
- Rindlisbacher MA, Weisberg MK, Ebel DS, Alpert SP (2021) Metal-rich nodules in anomalous EL3 chondrite Northwest Africa (NWA) 8785. *Meteorit Planet Sci* 56:960–970
- Rubin AE (1983) Impact melt-rock clasts in the Hvittis enstatite chondrite breccia: implications for a genetic relationship between EL chondrites and aubrites. *Proc Lunar Planet Sci Conf* 14:B293–B300
- Rubin AE, Scott ERD (1997) Abee and related EH chondrite impact-melt breccia. *Geochim Cosmochim Acta* 61:425–435
- Rubin AE, Huber H, Wasson JT (2009a) Possible impact-induced refractory-lithophile fractionations in EL chondrites. *Geochim Cosmochim Acta* 73:1523–1537
- Rubin AE, Griset CD, Choi B-G, Wasson JT (2009b) Clastic matrix in EH3 chondrites. *Meteorit Planet Sci* 44:589–601
- Sears DWG, Weeks KS, Rubin AE (1984) First known EL5 chondrite-evidence for dual genetic sequence for enstatite chondrites. *Nature* 308:257–259
- Trinquier A, Birk J-L, Allègre CJ (2007) Widespread ⁵⁴Cr heterogeneity in the inner Solar System. *Astrophys J* 655:1179–1185
- Trinquier A, Elliott T, Ulfeck D, Coath C, Krot AN, Bizzarro M (2009) Origin of nucleosynthetic isotope heterogeneity in the solar protoplanetary disk. *Science* 324:374–376
- van Achterberg E, Ryan CG, Jackson S, Griffin WL (2001) Data reduction software for LA-ICP-MS. In: Sylvester P (ed) *Laser-ablation-ICPMS in the earth sciences, principles and applications*, vol 29, pp 239–243
- Wasson JT, Kallemeyn GW (1988) Compositions of chondrites. *Philos Trans R Soc Lond A* 325:535–544
- Weisberg MK, Kimura M (2012) The unequilibrated enstatite chondrites. *Chemie Erde* 72:101–115
- Weyrauch M, Horstmann M, Bischoff A (2018) Chemical variations of sulfides and metal in enstatite chondrites—introduction of a new classification scheme. *Meteorit Planet Sci* 53:394–415
- Wheelerlock MM, Keil K, Floss C, Taylor GJ, Crozaz G (1994) REE geochemistry of oldhamite-dominated clasts from the Norton County aubrite: igneous origin of oldhamite. *Geochim Cosmochim Acta* 58:449–458
- Wood BJ, Smythe DJ, Harrison T (2019) The condensation temperatures of the elements: a reappraisal. *Am Mineral* 104:844–856
- Zhang Y, Sears DWG (1996) The thermometry of enstatite chondrites: a brief review and update. *Meteorit Planet Sci* 31:647–655

Publisher's Note

Springer Nature remains neutral with regard to jurisdictional claims in published maps and institutional affiliations.

Submit your manuscript to a SpringerOpen® journal and benefit from:

- Convenient online submission
- Rigorous peer review
- Open access: articles freely available online
- High visibility within the field
- Retaining the copyright to your article

Submit your next manuscript at ► [springeropen.com](https://www.springeropen.com)